Surface Science 758 (2025) 122742

Contents lists available at ScienceDirect

Surface Science

journal homepage: www.elsevier.com/locate/susc

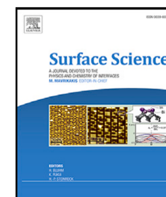

Electrical activity of aluminum, boron, and *n*-type impurities defect-complexes in germanium: Implications for enhanced Ge-based devices

Emmanuel Igumbor [a,*], Edwin Mapasha [b], Abdulrafiu Tunde Raji [c,d], Ezekiel Omotoso [e]

[a] Department of Electrical and Electronic Engineering Science, Faculty of Engineering and the Built Environment, University of Johannesburg, Johannesburg, South Africa
[b] Department of Physics, University of Pretoria, Pretoria 0002, South Africa
[c] The Executive Dean's Office, College of Science, Engineering and Technology, University of South Africa (UNISA), Florida 1709, South Africa
[d] National Institute of Theoretical and Computational Sciences (NITheCS), South Africa
[e] Department of Physics and Engineering Physics, Obafemi Awolowo University, Ile-Ife, 220005, Nigeria

ARTICLE INFO

Keywords:
Materials modeling
Semiconductor
Electronic
Defect-complexes
Ge
Defect-level

ABSTRACT

Studies on point defects in germanium (Ge) are increasing, primarily because these defects have the potential to modify the electronic and optical properties of Ge, thereby enhancing device applications. While significant progress has been made in defect studies, a comprehensive understanding of defect complexes resulting from interactions between *p*-type (Al or B) and *n*-type atoms ($D_{Ge}X_i$ and D_iX_{Ge}; where D = Al, B, and X = N, P, As, Sb) is still lacking. Therefore density functional theory calculations of electrically active defect levels in Ge that are caused by interactions between *n*-type impurity atoms and Al or B, are presented. For defect-complexes formed by Al and *n*-type atoms, Al and P exhibit the highest formation stability under equilibrium conditions. Conversely, $B_{Ge}P_i$ represents the most energetically favorable defect-complex. With the exception of $B_{Ge}N_i$, the energetic stability of all defect-complexes suggests that Al and B interstitials form strong bonds with *n*-type substitutional atoms. Electrical behavior analyses of these defects reveal that defect-complexes formed by Al and *n*-type atoms induce deep defect levels. Specifically, $Al_{Ge}N_i$ acts as an acceptor, while Al_iAs_{Ge} behaves as a donor. The defects $B_{Ge}Sb_i$, B_iP_{Ge}, and B_iAs_{Ge} donate electrons to the conduction band at energy levels within the range of 3 k_BT. Furthermore, $B_{Ge}Sb_i$ induces shallow donor levels, whereas $B_{Ge}P_i$ induces acceptor levels. This study opens new research opportunities in the experimental synthesis of defects and offers insights into controlling them, potentially enhancing electronic devices.

1. Introduction

Ge is a high-*k* material with superior charge carrier mobilities for both electrons and holes, leading to higher drive currents compared to silicon [1–4]. These significant properties provide Ge with a competitive advantage over Si in its potential role as a replacement for SiO_2 in highly scaled metal–oxide–semiconductor field-effect-transistors (MOSFETs) [5–7]. However, there is still a need to achieve *n*-type ultra-shallow junctions with a downsizing capability to 15 nm. Currently, this presents a challenge as downscaling necessitates doping levels as high as 10^{20} cm^{-3}. Several research studies have been conducted, focusing on the realization of Ge-based MOSFETs [5–7]. A new design has been proposed to enhance the performance of double-gate junction-less MOSFETs by incorporating a germanium channel [1]. However, the impact of defects, if not controlled, presents a challenge in realizing a Ge-based MOSFETs.

Doping germanium with heavy metals and impurities is crucial for enhancing its performance in microelectronics, optoelectronics, infrared, and fiber optics applications [8,9]. However, this process entails certain compromises due to the modulation of germanium's electronic and optical properties. The activation of *n*-type dopants, such as antimony, is essential to achieve n^+/p germanium diodes. This can primarily be employed for source/drain regions in Ge *n*-MOSFETs during the scaling process [10]. The results of ion implantation and melting laser thermal annealing indicate that doping Ge with *n*-type arsenic at a concentration of 1×10^{20} cm^{-3} could result in defect metastability [11]. Sb is reported to be capable of forming shallow junctions in Ge. However, when heavier ions are introduced into Ge through ion implantation at high doses, it can lead to severe surface damage [12]. A notable example is when Ge is doped with In, Bi, and Sn at high doses through implantation, which results in severe crystal damage at the surface, potentially impacting the performance

* Corresponding author.
E-mail address: elgumuk@gmail.com (E. Igumbor).

https://doi.org/10.1016/j.susc.2025.122742
Received 7 November 2024; Received in revised form 18 March 2025; Accepted 20 March 2025
Available online 29 March 2025
0039-6028/© 2025 The Authors. Published by Elsevier B.V. This is an open access article under the CC BY license (http://creativecommons.org/licenses/by/4.0/).

of devices [13]. *n*-type heavy doping in Ge with ultra-low resistivity using Sb deposition and pulsed laser melting has been documented in a study by Carraro et al. [14]. The combination of deposition techniques, such as sputtering or evaporation, for Sb followed by pulsed laser melting has been demonstrated to yield both high incorporation levels and improved dopant concentrations, reaching up to 3×10^{20} cm^{-3}. Moreover, ion implantation of Sb into Ge crystals, along with laser annealing, has proven successful in achieving an electrically active Sb concentration exceeding $2{\times}10^{20}$ cm^{-3}, as reported by Wahab et al. [10].

Studies on defect-complexes in semiconductors have been on the rise in recent times [15–23]. It has been established that these defects reside within their host materials in the form of complexes or clusters and may induce active electrical defect levels [24–29]. Studies on defect-complexes are not limited to only 3D or bulk materials. In 2D materials, various defect-complexes have been used to precisely tune the optical and electronic properties of emerging transition metal dichalcogenide materials [30–36]. In a recent theoretical analysis focused on the electronic properties and interactions of substitutional Mo defects within Mo-doped $BiVO_4$, it was discovered that these defect-complexes function as shallow donors, potentially enhancing the photoelectrochemical performance of the host material [37]. A recent study suggests that the interaction between V and As_i complexes leads to a decrease in dopant activation in GeSn [38]. Notably, the presence of Sn did not impede the formation of larger VAs_i complexes, thereby failing to mitigate donor deactivation [38].

In Ge, Si, diamond, GaAs, and GaN, AlN numerous defect-complexes have been reported [39–45]. The NV center in diamond and SiC is a well-known defect-complex with significant potential applications in state-of-the-art quantum information systems [46,47]. The formation of defect-complexes contributes to the *n*-type behavior and low doping efficiency of transparent conductive oxides and corresponds to deep traps [48]. In β-Ga_2O_3, divacancy-cation and interstitial-complexes serve as compensating acceptors [21]. The introduction of Sn facilitates the formation of divacancy-interstitial complexes, increasing the Fermi level energy and the vacancy concentration [21]. In GaN, the interaction between Mg_{Ga} and nitrogen vacancy induces defect levels that act as non-radiative electron–hole recombination centers, potentially leading to the production of a broad photoluminescence band at 1.76 eV [49]. Double nitrogen vacancies in GaN have low formation energies and act as efficient donors, generating two deep donor levels. This phenomenon could limit n/p-type doping and the minority carrier lifetime of the host semiconductor [50].

In the case of Ge, various defect-complexes have also been extensively studied [18,24,25,51]. Studies focusing on the interactions of primary defects with group-III and group-V impurities, which are often used for doping Si and Ge, have been reported in the literature [24, 52]. Additionally, these studies demonstrate how the concentration of shallow donor or acceptor states decreases due to irradiation [24, 52]. In the case of arsenic-doped Ge, it acts as a dominant trap at 300 K and forms clusters of defects that may include vacancies and dopants [53]. Furthermore, study on P-doped Ge suggests that two competing defect-complexes are involved in positron trapping, with complexes containing fewer P atoms exhibiting lower positive charge states [53]. In Ge, trivalent defect-complexes like $In_{Ga}In_i$ serve as recombination centers during the transition from charge state +1 to 0 [54]. Conversely, $Al_{Ga}Al_i$ acts as a donor, contributing electrons to the conduction band. Additionally, $B_{Ga}B_i$ exhibits characteristics of deep defect levels [54]. Despite these breakthroughs, there are still several defect-complexes whose compositions and their influence on the electrical properties of Ge remain poorly understood. For example, the electrically active defect levels induced by the interactions of Al or B with *n*-type atoms have not yet been thoroughly studied. In this report, we have provided theoretical insights that will assist in the experimental understanding of defect processes in Ge-based devices.

The aim of this study is to demonstrate how the interactions between Al or B and *n*-type impurity atoms can influence the structural, electronic, and electrical properties of Ge. In this study, we employed the screened Heyd, Scuseria, and Ernzerhof (HSE06) hybrid functional [55] within density functional theory (DFT) to predict the stability and formation of Al, B, and *n*-type impurity interactions, resulting in substitution-interstitial defect-complexes in Ge. Furthermore, we assessed the impact of these defects on the electronic properties of Ge. Our findings indicate that under equilibrium conditions, the defect-complexes formed due to the interactions of Al, B, and *n*-type atoms are energetically favorable. The agglomeration of defect-complexes, as determined by their binding energies, is stable, with external atoms readily forming bonds with the host atoms. Additionally, our results show that while the double donor defect levels induced by the interaction of Al and *n*-type atoms act as recombination centers, $B_{Ge}Sb_i$ behaves as a shallow donor defect. The findings from this study will provide valuable and unique insights for the experimental characterization of defect-complexes during device fabrication.

This paper is organized as follows: Section 2 presents the computational details, while Section 3 includes the results and discussions covering the formation, stability, and defect levels induced by the studied defect-complexes. Finally, Section 4 presents the conclusion.

2. Computational details

Density functional theory calculations using the Vienna *ab-initio* Simulation Package (VASP) [56] were performed. The core and chemically active electrons where separated using the projector-augmented wave (PAW) method [57]. The hybrid functional of the HSE with the Perdew, Burke and Ernzerhof (PBE) [58] were used as the exchange correlation. The hybrid functional approach is a combination of the PBE and the non-local Fock [55]. In this approach, mixing parameter and adjustable parameter needs to be converged with respect to the band gap. Considering the experimental band gap of Ge, the mixing and adjustable parameters of 25% (fraction of exact Hartree–Fock exchange) and 0.2 $Å^{-1}$, respectively were sufficiently used to predict a band gap of 0.78 eV, which is in agreement with the experimental band gap reported in Ref. [59]. Having obtained the appropriate HSE parameters, we constructed a supercell with 64 atoms and performed a geometric optimization using a Monkhorst–Pack [60] k-point of $2 \times 2 \times 2$ to sample the Brillouin zone. The energy cutoff was set to 400 eV, the minimum total energy convergence criteria was set to 10^{-6} eV and the forces acting on each of the atoms was less than 0.001 eV/Å . Spin orbit coupling was included in all calculations. The electronic properties calculations were performed with a denser k-points of $16 \times 16 \times 16$.

The formation energy calculations were performed from a well established formalism [61]. For instance, the formation energy ($E^F(B_{Ge}P_i, q)$) of a defect-complex of boron interstitial and phosphorus substitutions (B_iP_{Ge}) in charge state q is given as

$$E^F(B_{Ge}P_i, q) = E^{total}(B_{Ge}P_i, q) - E^{total}(Ge) + \triangle n_i \sum_i \mu_i + q[E_V + \varepsilon_F] + E^q_{FNV}, \quad (1)$$

where the total energies of the pristine Ge supercell and B_iP_{Ge} are $E^{total}(Ge)$ and $E^{total}(B_iP_{Ge}, q)$, respectively. The μ_i is the chemical potential of the type *i*th constituent atom. The number of atoms remove or added is represented by $\triangle n$. *n* becomes negative if an atom is added or positive if an atom is removed. The criteria for calculating the chemical potential of Ge atom and its value were taken from Ref. [62].

The chemical potential of each impurity atom was calculated from the most stable phase of each of the atoms. In DFT the chemical potential is obtained by evaluating the change in energy that is associated with the addition or removal of an atom. In this study, the rhombohedral structure which is the most stable phase of Sb and As was used for the chemical potential calculation. The chemical potentials of the Sb and As systems were calculated as the total energy of the system per the number of atoms. Similarly, for Al and B, the most stable phases are the face-centered cubic structure and the β-boron rhombohedral phase, respectively. Consequently, their chemical potentials were calculated as

the total energy per number of atoms [63]. In Eq. (1), the E_V and ε_F are the valence band maximum (VBM) and Fermi energy, respectively. The ε_F is varied from the VBM (zero) to the conduction band minimum (CBM) at 0.78 eV.

When a supercell method is employed for the modeling of defects (for instance, charge defects calculations), errors due to finite-size effects and spurious interactions of charge states are imminent. The correction term E^q_{FNV} according to the method proposed by Ref. [64], was included to account for the errors that may arise as a result of finite-size effect and defect–defect interactions. The formation energies of other defect-complexes studied were calculating using the same approach as in Eq. (1). The higher the formation energy of Eq. (1) the lower the concentrations of the entire Ge system.

The induced defect levels of the defect-complexes are determine by calculating the charge state transition levels in the band gap of the host semiconductor. Reports have show that, depending on the position of the Fermi level in the band gap, most point defects can be thermodynamically charge state stable in several different charge states [65]. The charge state transition level is an important electrical property of a defective semiconductor [65]. The position of the Fermi level could determine the defect-induced states within the band gap. For example, as the Fermi level is raise from the VBM, defect-induced states in the band gap may be filled with electrons [65]. Theoretically, the Fermi energy where there is an intersection of two different charge states is called the charge state transition energy level. The procedure of calculating the thermodynamic transition levels are detailed in Ref. [25, 54]. In defects studies, beside the isolated defects, there is possibility of the formation of two or more different defects to form a complex defect. The formed defect-complex stability could be understood from the binding energy. The binding energies of the defect-complexes were calculated using the method of Ref. [25,54].

3. Results and discussion

This section provides a comprehensive analysis and discussion of the interactions between Al and the *n*-type impurity, as well as the interactions between B and the *n*-type dopants in Ge. The electronic properties, formation energies and binding energies of the defect-complexes, exploring their implications were presented. Furthermore, a comparison of the electrically active characteristics of defect levels arising from the interactions between B, Al, and the *n*-type impurities were discussed.

Defects in a crystal are randomly distributed in a solid crystal structure. For defect-complexes, defects of different types may be close to each other or separated far away [54]. In Ref. [66] insights on how the most suitable defect sites have been identified when dealing with defect-complexes in Ge have been documented. In this study we have considered various defect-complexes configurations. We examined the impurity atoms both as nearest neighbors and at when they are separated from each other. Numerous defect sites were analyzed. Following an initial evaluation based on the total minimum energy results, we selected the configurations with the lowest total minimum energy. These included configurations with nearest-neighbor and second nearest-neighbor defect positions. Further investigations revealed that the nearest-neighbor defect complex is the most energetically favorable [54,66]. Consequently, in this study, we focused on exploring defect configurations in the nearest-neighbor scenario.

3.1. Defect-complexes formed by the Al and the *n*-type atoms in Ge

3.1.1. Structural properties of Al and the *n*-type atoms defect-complexes in Ge

Fig. 1 displays the relaxed geometry structures of the pristine Ge, Al_iAs_{Ge}, $Al_{Ge}P_i$, Al_iN_{Ge}, $B_{Ge}As_i$ and B_iAs_{Ge}. The bond lengths of the impurity atoms with Ge are shown in Table 1. The bond length between Ge and substitutional Al atoms ranges from 2.37 to 2.41 Å, which is slightly shorter than the Ge-Ge bond length of 2.46 Å. Additionally, the bond lengths formed by the interactions of substitutional and interstitial atoms significantly differ from the bond length of pristine Ge-Ge. For instance, the differences between the bond lengths of X_i-X_{Ge} and Ge-Ge are 0.63, 0.61, 0.14, 0.03, 0.06, and 0.14 Å, for N_iAl_{Ge}, Al_iN_{Ge}, $Al_{Ge}P_i$, $P_{Ge}Al_i$, $Al_{Ge}As_i$ and Al_iAs_{Ge}, respectively. The Ge crystal experiences increased strain due to the introduction of Al and *N* into its lattice. This strain may influence the formation energy of defect-complexes during formation. The preference of atoms to form bonds with their nearest neighbor atoms for the N_iAl_{Ge} and Al_iN_{Ge} was examined. For the interactions between *N* and Al, bond length strain is strong in the Ge crystal due to the bond length formed by Al-N. Furthermore, the interaction between Al atoms and Ge atoms induces less strain in the Ge crystal. This is because Al atoms have a preference for forming bonds with Ge atoms. For instance, regardless of whether the Al atom occupies an interstitial or substitutional position in the crystal structure, the bond length difference between Al-Ge and Ge-Ge is relatively smaller compared to the bond length difference between N-Ge, whether *N* is an interstitial or substitutional atom.

Table 1
The bond length of the nearest neighbor Al atom with Ge and n-type impurity atoms.

Atoms	$Al_{Ge}N_i$	Al_iN_{Ge}	$Al_{Ge}P_i$	Al_iP_{Ge}	$Al_{Ge}As_i$	Al_iAs_{Ge}
X_i-X_{Ge}(Å)	1.83	1.85	2.32	2.49	2.40	2.60
Ge-X_{Ge} (Å)	2.41	1.99	2.40	2.46	2.37	2.51
Ge-X_i (Å)	1.84	2.38	2.38	2.57	2.45	2.58

For the defect-complexes formed by the interactions of Al and P, the bond length of substitutional atoms with Al or P is very close to that of Ge-Ge. For instance, while the bond length difference between Ge and substitutional Al is 0.06 Å, there is no difference between the bond lengths of Ge-P and pristine Ge-Ge. However, the bond lengths of Ge and interstitial Al and P atoms significantly differ by 0.08 and 0.11 Å, for Ge-P and Ge-Al, respectively. For the $Al_{Ge}As_i$ and Al_iAs_{Ge}, we observed that the difference in bond length between As-Al and Ge-Ge is relatively smaller when the As atom occupies an interstitial or substitutional site, indicating a preference for the As atom to form a bond with the Ge atom. However, when Al occupies interstitial or substitution positions, significant lattice distortion occurs in the Ge crystal. In a defective system, the amount of strain induced by the impurity atoms can influence the energy required for such defects to form. Hence, in this study, we will demonstrate that defect-complexes with *N* may form with relatively higher formation energy, potentially impacting their ability to agglomerate into clusters.

3.1.2. Partial density of states of Al and the *n*-type atoms defect-complexes in Ge

The band gap result that was obtained for this study is in agreement with other theoretical and experimental results [65]. For instance, while the experimental band gap for Ge is 0.78 at 0 K, the GGA and LDA show a band gap of 0 eV. However, the implementation of the HSE provided an improved band gap of 0.78 eV [65].

Fig. 2 displays the partial density of states (PDOS) of pristine Ge. For the Ge system, its Fermi level is close to the valence band. Fig. 3 displays the plots of PDOS for the Al and *n*-type atoms defect-complexes in Ge. The Fermi level of Ge due to the $Al_{Ge}N_i$, $Al_{Ge}As_i$, and Al_iN_{Ge} is pinned to the valence band. This suggests that these defect-complexes modified the Ge system, and the end result is *p*-type semiconductors. The valence band of the $Al_{Ge}N_i$, $Al_{Ge}As_i$, and Al_iN_{Ge} is dominated by the *p*-orbital of impurity atoms; irrespective of whether the impurity atoms are interstitial or substitutional. However, the Al_iN_{Ge} and $Al_{Ge}N_i$ modulate the Ge system to behave as *n*-type semiconductor. The Fermi level of the Al_iN_{Ge} and $Al_{Ge}N_i$ is located inside the conduction band. Exhibiting a deep defect behavior. The $Al_{Ge}P_i$ induced multiple states deep in the mid-gap. These states are predominately contribution from the *p* and *s* orbitals of both Al and P atoms. As shown in Fig. 3, there is evidence of strong orbital hybridization between the Ge-*p* orbital and

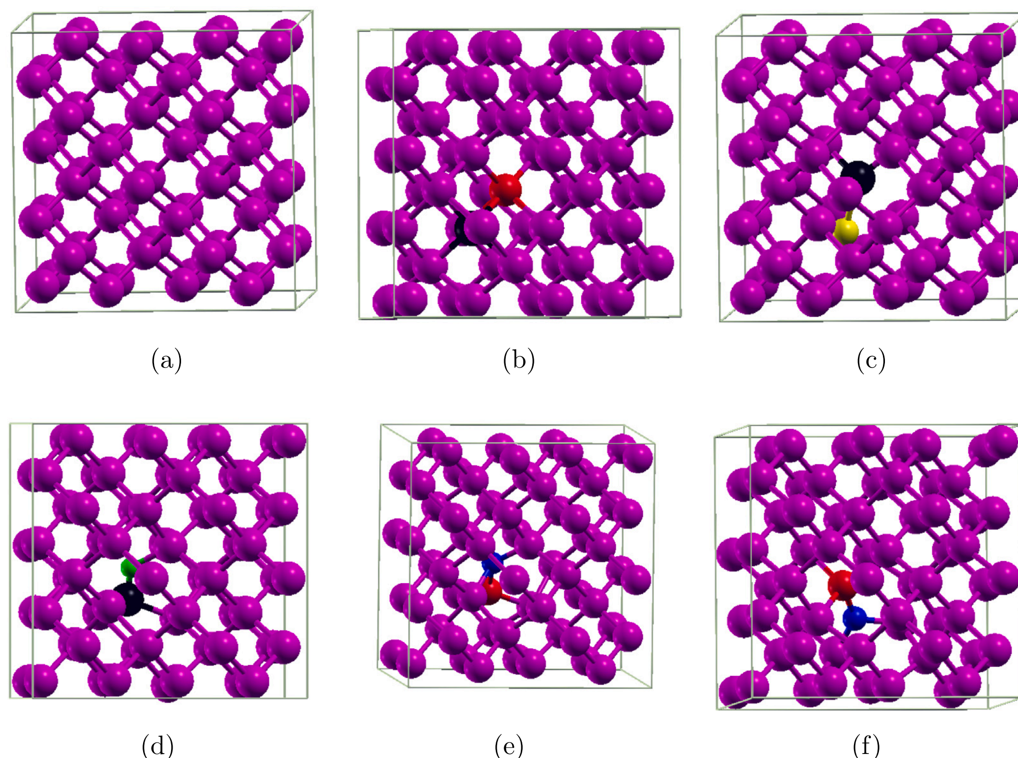

Fig. 1. The relaxed geometric structures of (a) pristine Ge, (b) Al_iAs_{Ge}, (c) $Al_{Ge}P_i$, (d) Al_iN_{Ge}, (e) $B_{Ge}As_i$ and (f) B_iAs_{Ge}. Ge, Al, B, P, As and *N* atoms are presented by purple, black, blue, yellow, red and green balls, respectively.

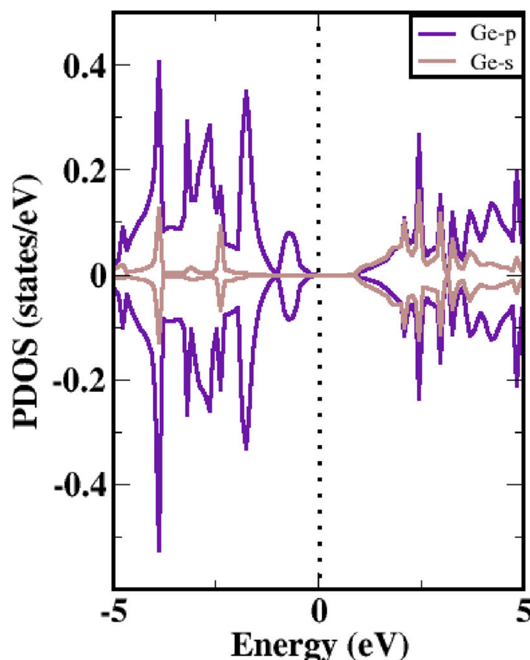

Fig. 2. The plot of partial density of states (PDOS) pristine Ge. The dash vertical line represents the Fermi level.

the *p*-orbital of all the impurities atoms in all the defect-complexes considered. The *s*-orbital of the Al atom dominates the VBM of the Al_iP_{Ge} and $Al_{Ge}As_i$. In additional, The impurity atoms play a dominant role in populating the conduction band edge. For instance, the *s* and *p* orbitals of As atom dominate the gap of the host material (Ge). A comparison of the PDOS of the defect-complexes and that of the pristine Ge shows strong influence of the external impurity atoms on the host, resulting in the additional creation of states.

3.1.3. Formation and binding energies of Al and n-type atoms defect-complexes in Ge

In this section, we presented results of the formation of six different defect-complexes resulting from the interactions between aluminum and *n*-type atoms. Table 2 displays the formation and binding energies of these defect-complexes. The formation energies of $Al_{Ge}P_i$, Al_iP_{Ge}, $Al_{Ge}As_i$, and Al_iAs_{Ge} are all less than 6.20 eV, while those of $Al_{Ge}N_i$ and Al_iN_{Ge} are relatively high. Under thermodynamic equilibrium conditions, the $Al_{Ge}P_{Ge}$ with an energy of 5.13 eV is the most energetically favorable defect-complex. With the exception of the $Al_{Ge}N_i$ and Al_iN_{Ge}, the formation energies of all defect-complexes are lower than the formation energy of di-interstitials in Ge [62]. The order of increase in the formation energy of the interactions of the Al and *n*-type atoms is $Al_iP_{Ge}<Al_{Ge}P_i<Al_iAs_{Ge}<Al_{Ge}As_i<Al_iN_{Ge}<Al_{Ge}N_i$. The defect-complexes are more energetically favorable when Al acts as an interstitial atom and *n*-type atoms act as substitution atoms. The formation energies of defect-complexes formed by Al with *p*-type impurities range between 4.14 and 6.16 eV [24], while the formation energies of Al with *n*-type impurities range between 5.13 and 11.66 eV. This indicates that the formation of defect-complexes formed by the interaction of Al with *p*-type atoms is more energetically favorable compared to those formed with *n*-type atoms. The amount of strain experienced by the Ge crystal due to external impurities is particularly high for defect-complexes formed with N. Consequently, this influences the amount of formation energy required for such defects to emerge.

The stability of defect-complexes was studied by calculating their binding energies. The $Al_{Ge}P_i$, Al_iP_{Ge}, $Al_{Ge}As_i$, and Al_iAs_{Ge} defect-complexes all have positive binding energies. This indicates that all the aforementioned defect-complexes are energetically stable when compared to their isolated, non-interacting defects. It also suggests that the interactions between Al/P and Al/As could lead to stable defect-complexes that should be experimentally synthesized. However, if they

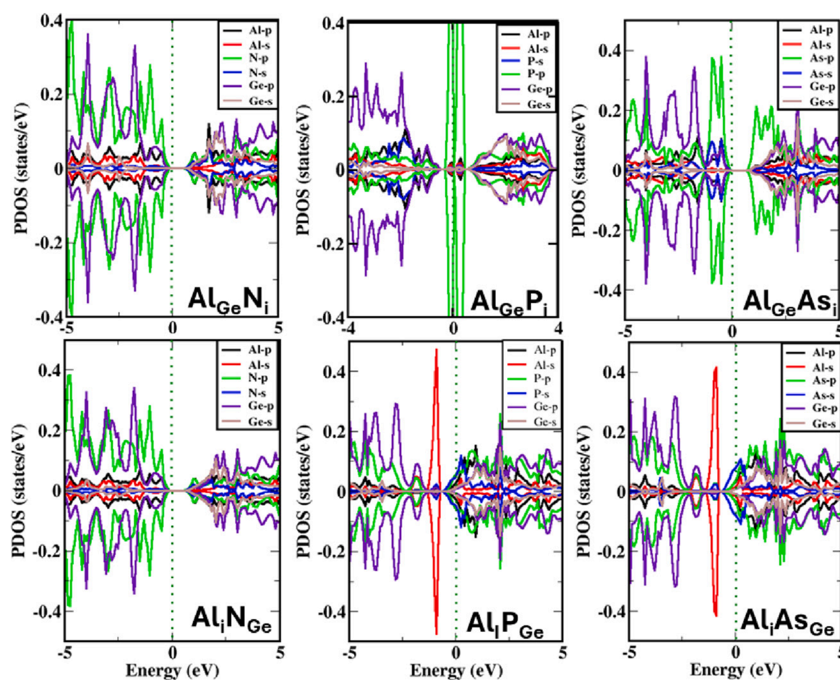

Fig. 3. The plot of partial density of states (PDOS) for Al and *n*-type atoms substitutional–interstitial pairs in Ge. The Fermi level positioned at 0 eV.

Table 2
The formation and binding energies of the defect complexes formed in Ge due to substitution-interstitial interactions between Al and *n*-type atoms. These energies are reported for the neutral charge state and calculated at zero Fermi energy.

Defect	Formation energy (eV)	Binding energy (eV)
$Al_{Ge}N_i$	11.66	−2.87
Al_iN_{Ge}	11.61	−0.96
$Al_{Ge}P_i$	5.40	3.20
Al_iP_{Ge}	5.13	1.72
$Al_{Ge}As_i$	6.19	3.54
Al_iAs_{Ge}	5.80	1.70

Table 3
The charge state transition energy levels ($\varepsilon(q/q')$) above the VBM in eV induced in Ge by the defect-complexes formed due to the interactions between Al and the *n*-type interstitial and substitutional pairs.

Defect	(+2/ + 1)	(+1/0)	(0/ − 1)	(−1/ − 2)
$Al_{Ge}N_i$	–	–	0.20	0.44
Al_iN_{Ge}	0.33	0.60	0.71	–
Al_iP_{Ge}	0.61	–	–	–
$Al_{Ge}P_i$	0.20	0.35	0.50	0.66
$Al_{in}As_{Ge}$	0.60	–	–	–
$Al_{Ge}As_i$	0.54	0.66	0.77	–

were to dissociate, it would likely require an energy expense higher than their respective formation energies. The $Al_{Ge}N_i$ and Al_iN_{Ge} defect complexes have high formation energies. Their relatively negative binding energies suggest the possibility of the defect to decompose into non-interacting defects at an energy lower than their respective formation energies. Such defect-complexes, if intended to form, will split with an energy lower than their formation energies. Under thermodynamic equilibrium conditions, the $Al_{Ge}P_i$ and $Al_{Ge}As_i$ defect-complexes are the most stable, with binding energies of 3.20 and 3.54 eV, respectively.

3.1.4. Defect levels induced by Al and the n-type atoms defect-complexes in Ge

Defects in semiconductors may exhibit electrically active defect levels that depend on their charge states [65]. In this study, we predicted the electrically active defect levels induced by the interactions between Al and *n*-type impurity atoms in Ge. Table 3 lists the charge state transition defect levels of defect-complexes in Ge. The plots of the formation energy as a function of the Fermi energy for Al and the *n*-type atoms defect-complexes in Ge are shown in Fig. 4.

The $Al_{Ge}N_i$ behaves as an acceptor, inducing both single ((0/−1)) and double ((−1/−2)) acceptor defect levels in the band gap of Ge (see Fig. 4(a)). The (0/−1) and (−1/−2) defect levels are deep centers located at E_V +0.20 and E_V +0.44 eV, respectively. All the defect levels induced by $Al_{Ge}N_i$ have the potential to act as recombination centers. As shown in Fig. 4(b), the Al_iN_{Ge} induces three distinct defect levels in Ge: (+2/+), (+1/0), and (0/−1). This suggests that Al_iN_{Ge} can act as either a donor or acceptor, depending on its position within the band gap. For instance, when the defect level is significantly distant from the valence band, the double donor state is the most thermodynamically stable at E_V +0.33 eV. However, as the Fermi level approaches the conduction band, around an energy level of 0.60 eV, Al_iN_{Ge} undergoes a charge state transition from a double donor to a single donor state. Furthermore, as the Fermi level approaches the conduction band, reaching 0.07 eV below the conduction band, Al_iN_{Ge} switches to an acceptor defect, exhibiting single acceptor characteristic.

The $Al_{Ge}P_i$ and Al_iP_{Ge} exhibit different characteristics in terms of their defect levels (see Figs. 4(c) and 4(d)). The Al_iP_{Ge} induces a donor defect level, with the (+2/+1) defect level located at an energy of E_C-0.17 eV. On the other hand, the $Al_{Ge}P_i$ induces four distinct defect levels: (+2/+1), (+1/0), (0/−1), and (−1/−2). These defect levels are located at E_V+0.20 eV, E_V+ 0.35 eV, E_V+0.50 eV and E_C-0.12 eV, respectively. The (−1/−2) defect level can act as either a deep or shallow defect level, depending on the temperature. The majority of the defect-levels induced by the $Al_{Ge}P_i$ can act as recombination centers. Hence, they have the potential to diminish the lifespan of charge carriers, consequently lowering the overall effectiveness of Ge-based devices.

While the $Al_{Ge}As_i$ as shown in Fig. 4(e) functions as both a donor and an acceptor defect, depending on the locations of its Fermi level, the Al_iAs_{Ge} behaves as a donor (see Fig. 4(f)). The sole defect level induced by Al_iAs_{Ge} is deep and positioned at E_C-0.18 eV. This energy level is inadequate for electrons to make the transition into the conduction band. If such a transition were to occur, it would necessitate

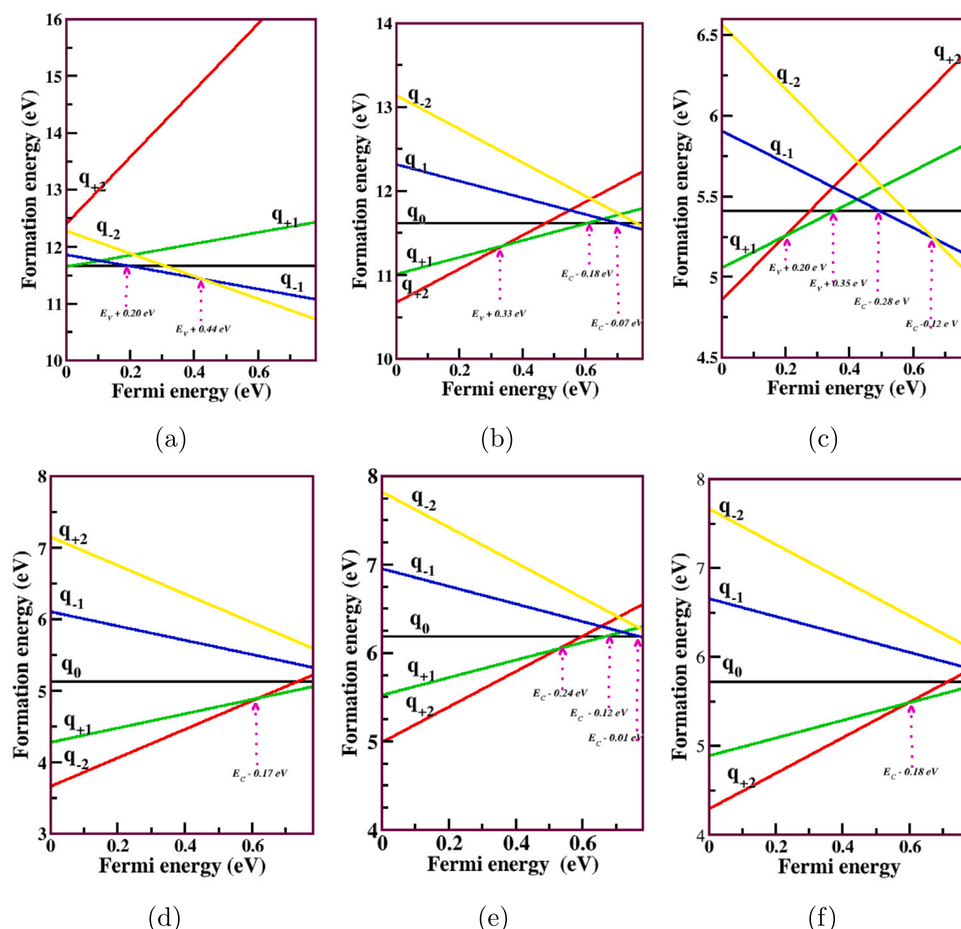

Fig. 4. The plots of formation energy as a function of the Fermi energy for: of (a) $Al_{Ge}N_i$, (b) Al_iN_{Ge}, (c) $Al_{Ge}P_i$, (d) Al_iP_{Ge}, (e) $Al_{Ge}As_i$ and (f) Al_iAs_{Ge}.

Table 4
The bond length of the nearest neighbor B atom with Ge and n-type impurities atoms.

Atoms	B_iN_{Ge}	$B_{Ge}N_i$	$B_{Ge}P_i$	B_iP_{Ge}	$B_{Ge}As_i$	B_iAs_{Ge}	$B_{Ge}Sb_i$	B_iSb_{Ge}
X_i-X_{Ge}(Å)	1.40	1.46	1.85	1.85	1.96	1.96	2.20	2.34
Ge-X_{Ge} (Å)	1.95	2.12	2.37	2.04	2.06	2.46	2.05	2.63
Ge-X_i (Å)	2.04	1.88	1.95	2.34	2.36	1.94	2.67	2.00

additional energy. Given that this energy level is higher than approximately 3 *k*T (thermal energy), it is more probable for this donor level, situated around 0.18 eV below the CBM, to promote recombination center.

The defect levels induced by $Al_{Ge}As_i$ are distributed throughout the band gap of Ge. The double donor defect level associated with $Al_{Ge}As_i$ is deep, positioned at 0.54 eV from the valence band, thereby promoting recombination processes. In contrast, the single acceptor level induced by $Al_{Ge}As_i$ is shallow, nearly aligned with the CBM. Furthermore, the single donor defect level (+1/0) of $Al_{Ge}As_i$ is located at E_C-0.12 eV. This implies that at higher temperatures, this defect level may shift closer to the CBM, allowing it to donate electrons. However, under equilibrium conditions and at low temperatures, the (+1/0) defect level may serve as a recombination center.

3.2. Defect-complexes formed by B and *n*-type atoms, substitutional–interstitial pairs in Ge

3.2.1. Structural properties of B and *n*-type atoms, substitutional–interstitial pairs in Ge

Table 4 lists the bond lengths of the nearest neighbor impurity atoms with Ge, ranging between 1.40–2.31 Å. The difference in bond lengths between impurity atoms and Ge-Ge slightly increases in this order- Sb<As<P<N. This indicates that the interaction between B and *N* may induce more strain in the Ge crystal. Comparing the bond length between B-N and Ge-Ge, the differences are 1.06 Å and 1.00 Å for the B_iN_{Ge} and $B_{Ge}N_i$ defect-complexes, respectively. Conversely, the difference between the bond lengths of B-Sb and Ge-Ge is 0.26 Å and 0.12 Å for the $B_{Ge}Sb_i$ and B_iSb_{Ge} complexes, respectively. The bond lengths between Ge and interstitial atoms range from 2.67–1.88 Å. The bond length of the B-N is the lowest, while that of the B-Sb is the highest. Despite the longer bond length of the B-Sb, the B-N induce more strain in the Ge system. For instance, the differences between the bond lengths of Ge-Ge and B-N(B-S) is 0.58 Å (0.21 Å). The bond lengths between Ge and substitutional atoms show variations, with B-N having the shortest bond length and B-Sb the longest. Our results showed that a B atom can easily form bond with Ge resulting in less strain compared to the *N* atom. This is regardless of their lattice site. Similarly, the interaction of B and P atoms induces more strain in the Ge crystal, leading to higher bond lengths for the Ge-P or Ge-B compared to Ge-Ge bonds. This trend is also observed for the B-As interactions, although Ge tends to form more stable bond lengths with As in contrast to with B.

3.2.2. Partial density of states of B and the *n*-type atoms defect-complexes in Ge

The PDOS of the B and *n*-type atoms defect-complexes in Ge are displayed in Fig. 5. The $B_{Ge}N_i$, B_iP_{Ge}, $B_{Ge}P_i$, $B_{Ge}As_i$, B_iAs_{Ge}, and $B_{Ge}Sb_i$ behave as *p*-type semiconductors. Their band gaps are populated by the *p*-orbital of the interstitial impurity atoms. For the B_iN_{Ge}, the Fermi level is filled with orbital states from the impurity atoms (*s*-orbitals of both *N* and B atoms and *p*-orbital of *N* atoms). The B_iN_{Ge}

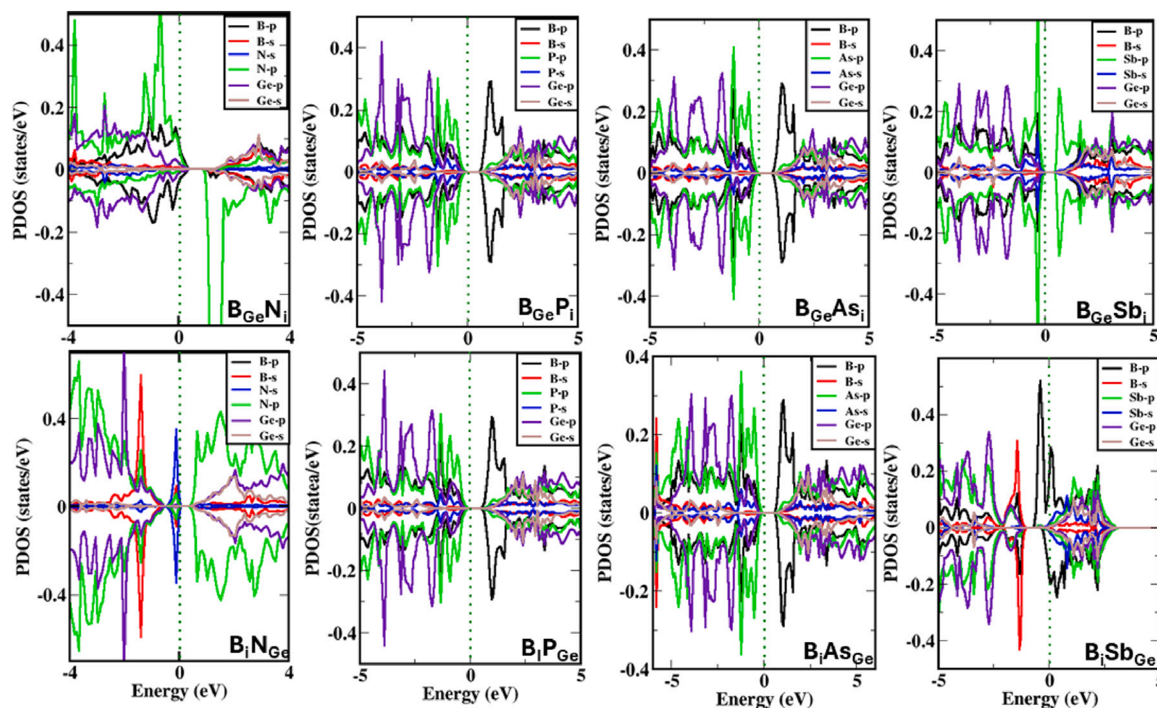

Fig. 5. The plot of partial density of states (PDOS) for B and *n*-type atoms substitutional–interstitial pairs in Ge. Note, the Fermi level is set to 0 eV.

Table 5
The formation and binding energies of the defect-complexes formed by the interactions between the substitution and interstitial of the B and the *n*-type atoms in Ge. The displayed energies are for the neutral charge state and calculated at zero Fermi energy.

Defect	Formation energy (eV)	Binding energy (eV)
$B_{Ge}N_i$	11.90	−1.12
B_iN_{Ge}	11.72	0.47
$B_{Ge}P_i$	5.79	4.80
B_iP_{Ge}	7.99	0.41
$B_{Ge}As_i$	6.02	5.70
B_iAs_{Ge}	8.16	0.81
$B_{Ge}Sb_i$	8.59	5.65
B_iSb_{Ge}	7.21	1.63

induced states at the conduction band are asymmetric, suggesting evidence of spin polarization. In all the B and *n*-type atoms defect-complexes examined, there is strong orbital hybridization between the participating *p*- and *s* orbitals of the external impurity and host atoms. As shown in Fig. 5, the *p*-type semiconductor-like systems exhibit localized states induced in Ge by the defects, which, in this case, result from the substitutional and interstitial impurities of the *n*-type atoms. Whereas B_iSb_{Ge} behaves as an *n*-type semiconductor, its Fermi level is pinned to the conduction band, with a strong influence of spin polarization. Furthermore, the *s*-orbital of the B atom dominates the valence band, while the *p*-orbital of the B atom dominates the CBM. The B_iSb_{Ge}-induced ground-state orbitals are broad, exhibiting significant delocalized states. A comparison of the pristine Ge, B and the *n*-type atom defect-complexes PDOS reveals a significant number of additional states in Ge. This is expected; however, some of the induced states will influence the defect level type, either by positioning them near the VBM or creating mid-gap defect levels, as will be discuss later in this paper.

3.2.3. Formation and binding energies of B and n-type atoms substitutional–interstitial pairs in Ge

In order to predict the possibility of B and *n*-type defect-complexes in Ge, it is important to calculate their formation energies. The predicted formation and binding energies are displayed in Table 5. The defect-complexes with low formation energies include $B_{Ge}P_i$, $B_{Ge}As_i$, and B_iSb_{Ge}, with formation energies of 5.79, 6.02, and 7.21 eV, respectively. Nevertheless, $B_{Ge}N_i$ and B_iN_{Ge}, characterized by their high formation energies, represent the least energetically favorable defects, with respective formation energies of 11.90 and 11.72 eV. Interestingly, the interactions between B and P atoms, as well as B and As atoms, exhibit more energetically favorable conditions when an *n*-type impurity occupies the interstitial site, in contrast to when they are positioned at substitutional sites. It is worth noting that the formation energies of defect-complexes are influenced by the amount of strain experienced in the bonds between the impurity and host atoms.

A comparison between previous studies on defect-complexes formed by the interactions of B atoms with *p*-type atoms and this current study reveals that B atom tends to exhibit higher energetic favorability in forming defect-complexes with *p*-type atoms in contrast to *n*-type atoms. For example, the formation energies of defect-complexes resulting from the interaction of B atom with *p*-type atoms range between 5.43 and 6.35 eV [24]. Conversely, the formation energies of defect-complexes formed by the interaction of B atom with *n*-type atoms range between 6.02 and 11.90 eV.

To determine whether the defect-complexes will remain bound without dissociating into non-interacting smaller defects at energies lower than their formation energy, we calculated the binding energies of defect-complexes of B and *n*-type atom substitutional–interstitial pairs in Ge. The $B_{Ge}N_i$ defect-complex is not stable, suggesting a high probability of dissociation, especially at room temperature (300 K). In contrast, B_iN_{Ge} with a high formation energy of 11.72 eV, has a binding energy of 0.47 eV, indicating its stability. However, the chances of dissociation are minimal unless additional energy surpassing its formation energy is introduced. Other stable defect-complexes include $B_{Ge}P_i$, B_iP_{Ge}, $B_{Ge}As_i$, B_iAs_{Ge}, $B_{Ge}Sb_i$, and B_iSb_{Ge}. Among these, the $B_{Ge}As_i$ and $B_{Ge}Sb_i$ are the most stable defect-complexes.

3.2.4. Defect levels induced by the B and n-type atoms, substitutional–interstitial pairs in Ge

Defects, when present, may introduce additional eigenstates in the band gap of semiconductor. These states may be located near the conduction band, deep in the band gap, or close to the valence band. Table 6 displays the charge state transition energy levels of the B and

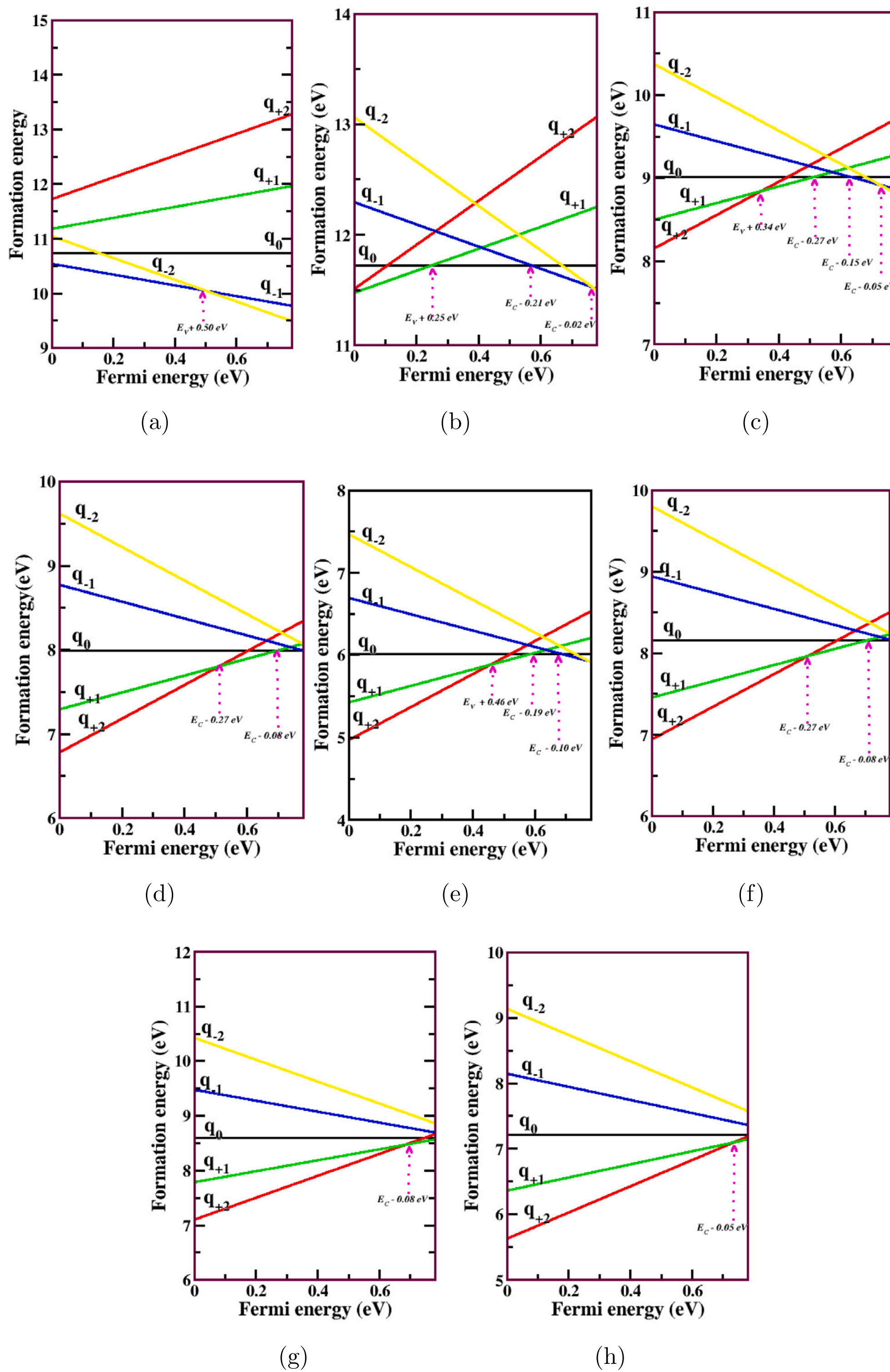

Fig. 6. The plots of formation energy as a function of the Fermi energy for: of (a) $B_{Ge}N_i$ (b) B_iN_{Ge}, (c) $B_{Ge}P_i$, (d) B_iP_{Ge}, (e) $B_{Ge}As_i$ (f) B_iAs_{Ge}, (g) $B_{Ge}Sb_i$, and (h) B_iSb_{Ge}.

n-type defect-complexes in Ge. The plots of the formation energy as a function of the Fermi energy for the defect-complexes are shown in Fig. 6. The $B_{Ge}N_i$ is an unstable defect-complex, making it challenging to predict its electrically active defect levels. However, such a defect-complex induced a deep defect level at E_V+0.50 eV (see Fig. 6(a)). The B_iN_{Ge} induces three distinct defect levels: (+1/0), (0/−1), and (−1/−2). Among these, the (+1/0) and (0/−1) are single and deep defects, while the (−1/−2) behaves as a shallow acceptor defect as shown in Fig. 6(b). The $B_{Ge}P_i$ defect-complex induced four distinct defect levels as shown in Fig. 6(c). These defect levels consist of both single and double donor, as well as single and double acceptor defects. While the (+2/+1), (+1/0), and (0/−1) are all deep defect levels that may serve as recombination centers, the (−1/−2) is a shallow acceptor defect with an energy level of E_C-0.05 eV. As displayed in Fig. 6(d), the B_iP_{Ge} induces double donor defect level. The (+2/+1) defect level is deep at E_V+0.51 eV, while the (+1/0) level is a shallow donor, at E_C-0.10 eV. Hence, at room temperature (300 K), the B_iP_{Ge} may donate electrons to the conduction band.

Table 6
The charge state transition ($\varepsilon(q/q')$) energy levels above the VBM in eV induced in Ge by defect-complexes formed due to the interactions between B and the *n*-type substitutional and interstitial atoms.

Defect	(+2/ + 1)	(+1/0)	(0/ − 1)	(−1/ − 2)
B_iN_{Ge}	–	0.25	0.57	0.76
$B_{Ge}N_i$	–	–	–	0.50
B_iP_{Ge}	0.51	0.70	–	–
$B_{Ge}P_i$	0.34	0.51	0.63	0.73
B_iAs_{Ge}	0.51	0.70	–	–
$B_{Ge}As_i$	0.46	0.59	0.68	–
B_iSb_{Ge}	0.73	–	–	–
$B_{Ge}Sb_i$	0.70	–	–	–

The $B_{Ge}As_i$ (Fig. 6(e)) induced two deep defect levels. The (+2/+1) defect level is positioned at E_V+0.46 eV. However, the (0/−1) acceptor level of E_C-0.10 eV is shallow close to the CBM. The B_iAs_{Ge} (Fig. 6(f)) acts as donor and induced two notable defect levels close to the conduction band (CB). The (+1/0) donor level of the B_iAs_{Ge} is located at E_C-0.08 eV, while its (+2/+1) level of is located at the energy level of E_C-0.27 eV. The $B_{Ge}Sb_i$ (Fig. 6(g)) and B_iSb_{Ge} (Fig. 6(h)) act as donors and induced defect levels close to the conduction band (CB). The (+2/+1) donor level of the $B_{Ge}Sb_i$ is located at E_C-0.08 eV, while the (+2/+1) level of $B_{Ge}Sb_i$ is located at the same energy level of E_V+0.70 eV. Finally, understanding the significance of deep defect levels is essential, as they may act as recombination centers during defect characterization. The recombination centers induced by defect-complexes in this study indicate they can capture charge carriers. Consequently, this scenario poses reliability concerns, including heightened susceptibility to radiation damage and accelerated aging.

The charge state transition levels induced by B atom and *n*-type defect complexes in Ge reveal intriguing defect levels that could be considered for enhancing device fabrication. Donor defect levels induced by these defect-complexes hold particular significance, especially when they are located close to the CBM. Notably, the donor defect levels of B_iP_{Ge}, B_iAs_{Ge}, and $B_{Ge}Sb_i$ are all in proximity to the conduction band. The single donor (+1/0) level of $B_{Ge}Sb_i$, in particular, is positioned just 0.08 eV below the conduction band. This implies that their ionization energy is within the range of 3 k_BT at 300 K. Due to this proximity to the conduction band, these defects can readily donate electrons to the conduction band, potentially generating free carriers of electricity.

3.3. Comparison between Al and B defect-complexes

Amongst the defect-complexes formed with *N* atom, all exhibit high formation energies. The formation energy in ascending order is as follows Al_iN_{Ge}< $Al_{Ge}N_i$< B_iN_{Ge}< $B_{Ge}N_i$. The B_iN_{Ge} in particular, can act as a recombination center due to its deep defect levels. While the $B_{Ge}N_i$ is an unstable defect, with a negative binding energy, the B_iN_{Ge} is a stable defect-complex. The defect levels induced by A_iN_{Ge} predominantly exhibit considerable deep donor characteristics, with the exception of a single acceptor level. For the interactions of P with B and Al atoms, it is discernible that the affinity of P for the Al atom is notably higher, making it the most energetically favorable interaction. This disparity in energy is attributed to the shared group affiliation between Al and P, resulting in a reduced energy requirement for bond formation compared to interactions involving the B atom. Moreover, the P atom demonstrates the capability to establish bonds with both Al and B atoms without undergoing dissociation at the expense of energy. Conversely, the As atom consistently maintains stability in its interactions with both Al and B atoms. Notably, while the As atom forms bonds with the Al atom with relatively low energy, bonding with the B atom necessitates a comparatively higher energy input. Nevertheless, the binding energies remain stable across all observed cases. The defect levels induced by the interactions of As, Al and B atoms show that the presence of As alongside Al ($Al_{Ge}As_i$) leads the formation of shallow acceptor and donor levels depending on the position of the Fermi energy while interaction with B induces shallow acceptor level (B_iAs_{Ge}). In contrast, Sb does not engage in bonding with Al. However, in the case of B, it forms bonds, resulting in the generation of only a donor defect level situated very close to the CBM for both the B_iSb_{Ge} and $B_{Ge}Sb_i$.

4. Conclusion

We used hybrid density functional theory to predict electrically induced defect levels resulting from the interactions between external atoms (Al, B) and *n*-type impurities, to form defect-complexes in Ge. We also predicted the electronic properties, formation energies and stabilities of these defect-complexes ($D_{Ge}X_i$ and D_iX_{Ge}, where D represents Al or B, and X represents N, P, As, or Sb. In the category of defect-complexes formed by the interactions between Al and *n*-type atoms ($Al_{Ge}X_i$ and Al_iX_{Ge}), we observed relatively low formation energies ranging from 5.40 to 11.66 eV. Under equilibrium conditions, the $Al_{Ge}P_i$ and Al_iP_{Ge} emerged as the most energetically favorable defect-complexes. Amongst these, the $Al_{Ge}P_i$ and $Al_{Ge}As_i$ have binding energies of 3.20 and 3.54 eV, respectively, making them the most stable defect-complexes. For the $B_{Ge}X_i$ and B_iX_{Ge} category, the $B_{Ge}P_i$ stood out as the most energetically favorable. With the exception of the $B_{Ge}N_i$, all defect-complexes in this category exhibited a high likelihood of forming strong bonds with host atoms in the presence of interstitial atoms. Defect levels resulting from the interactions of Al atom with *n*-type impurities in Ge exhibited characteristics of deep donor behavior. However, defect levels induced by Al_iN_{Ge} and $Al_{Ge}As_i$ shallow single acceptor, positioned near the conduction band minimum. In the context of interactions between B atom and *n*-type impurities in Ge, the defect-complexes revealed distinct behaviors. Specifically, the B_iAs_{Ge} and B_iP_{Ge} exhibited shallow single donor defect levels, whereas the double donor defect level of the $B_{Ge}Sb_i$ was positioned near the conduction band. Conversely, the (+1/0) and (0/−1) defect levels of B_iN_{Ge} and $B_{Ge}P_i$ appeared as deep defects, potentially serving as recombination centers. The results of this study offer theoretical insights into the characterization of defect-complexes arising from the interactions of external Al and B atoms with *n*-type impurities in Ge. The understanding of the defect-complexes formed by the Al, B, and *n*-type atoms in Ge is pivotal for device improvement. Furthermore, this study provides valuable insights into controlling deep defect levels and external defects during the fabrication of Ge-based devices.

CRediT authorship contribution statement

Emmanuel Igumbor: Writing – review & editing, Writing – original draft, Validation, Methodology, Investigation, Formal analysis, Data curation, Conceptualization. **Edwin Mapasha:** Validation, Supervision, Software, Resources. **Abdulrafiu Tunde Raji:** Visualization, Validation, Supervision, Software, Resources. **Ezekiel Omotoso:** Writing – review & editing, Writing – original draft.

Declaration of competing interest

The authors declare that they have no known competing financial interests or personal relationships that could have appeared to influence the work reported in this paper.

Acknowledgments

Emmanuel Igumbor is grateful to the University of Johannesburg, South Africa for funding. The authors appreciate the Center for High Performance Computing (CHPC) Cape Town, South Africa, for providing computational resources.

Data availability

Data will be made available on request.

References

[1] G. Dhiman, et al., Design and performance analysis of germanium-based junctionless double gate MOSFET, in: 2020 International Conference on Emerging Trends in Communication, Control and Computing, ICONC3, IEEE, 2020, pp. 1–4.

[2] A. Nayfeh, C.O. Chui, T. Yonehara, K.C. Saraswat, Fabrication of high-quality p-MOSFET in ge grown heteroepitaxially on Si, IEEE Electron Device Lett. 26 (5) (2005) 311–313.

[3] D. Brunco, B. De Jaeger, G. Eneman, J. Mitard, G. Hellings, A. Satta, V. Terzieva, L. Souriau, F. Leys, G. Pourtois, et al., Germanium MOSFET devices: Advances in materials understanding, process development, and electrical performance, J. Electrochem. Soc. 155 (7) (2008) H552.

[4] L. Lee, E.A. Fitzgerald, T. Bulsara, T. Currie, A. Lochtefeld, J. Appl. Phys. 97 (1) (2005) 011101.

[5] D.-B. Ruan, K.-S. Chang-Liao, Z.-Q. Hong, J. Huang, S.-H. Yi, G.-T. Liu, P.-C. Chiu, Y.-L. Li, Radiation effects and reliability characteristics of Ge pMOSFETs, Microelectron. Eng. 216 (2019) 111034.

[6] D. Yadav, D.R. Nair, Impact of source to drain tunneling on the ballistic performance of Si, Ge, GaSb, and GeSn nanowire p-MOSFETs, IEEE J. the Electron Devices Soc. 8 (2020) 308–315.

[7] W.-C. Wen, Y. Nagatomi, H. Akamine, K. Yamamoto, D. Wang, H. Nakashima, Interface trap and border trap characterization for Al2O3/GeOx/Ge gate stacks and influence of these traps on mobility of Ge p-MOSFET, AIP Adv. 10 (6) (2020) 065119.

[8] Y. Yang, S.-C. Liu, Z. Li, D.-J. Xue, J.-S. Hu, In-plane anisotropic 2D Ge-based binary materials for optoelectronic applications, Chem. Commun. (2021).

[9] D. Malo, A. Lizunova, A. Ramanenka, B. Masnaviev, V. Solovey, V. Ivanov, Near-infrared photoluminescence and micro-Raman study of spark discharge germanium nanoparticles, in: Journal of Physics: Conference Series, vol. 1695, (1) IOP Publishing, 2020, 012123.

[10] Y.A. Wahab, N. Soin, M.N. Naseer, H. Hussin, R.A.M. Osman, M.R. Johan, N.A. Hamizi, O.A. Pivehzhani, Z.Z. Chowdhury, S. Sagadevan, et al., Junction engineering in two-stepped recessed SiGe MOSFETs for high performance application, in: AIP Conference Proceedings, vol. 2203, (1) AIP Publishing LLC, 2020, 020033.

[11] R. Milazzo, G. Impellizzeri, D. Piccinotti, D. De Salvador, A. Portavoce, A. La Magna, G. Fortunato, D. Mangelinck, V. Privitera, A. Carnera, et al., Low temperature deactivation of Ge heavily n-type doped by ion implantation and laser thermal annealing, Appl. Phys. Lett. 110 (1) (2017) 011905.

[12] A. Satta, E. Simoen, T. Janssens, T. Clarysse, B. De Jaeger, A. Benedetti, I. Hoflijk, B. Brijs, M. Meuris, W. Vandervorst, Shallow junction ion implantation in Ge and associated defect control, J. Electrochem. Soc. 153 (3) (2006) G229.

[13] T. Janssens, C. Huyghebaert, D. Vanhaeren, G. Winderickx, A. Satta, M. Meuris, W. Vandervorst, Heavy ion implantation in Ge: Dramatic radiation induced morphology in Ge, J. Vac. Sci. Technol. B: Microelectron. Nanometer Struct. Process. Meas. Phenom. 24 (1) (2006) 510–514.

[14] C. Carraro, R. Milazzo, F. Sgarbossa, D. Fontana, G. Maggioni, W. Raniero, D. Scarpa, L. Baldassarre, M. Ortolani, A. Andrighetto, et al., N-type heavy doping with ultralow resistivity in Ge by Sb deposition and pulsed laser melting, Appl. Surf. Sci. 509 (2020) 145229.

[15] E. Bourgeois, M. Gulka, M. Nesladek, Photoelectric detection and quantum readout of nitrogen-vacancy center spin states in diamond, Adv. Opt. Mater. 8 (12) (2020) 1902132.

[16] S.A. Aravindh, I.S. Roqan, H. Alawadhi, Density functional theory studies of Zn 12 O 12 clusters doped with Mg/Eu and defect complexes, J. Cluster Sci. (2020) 1–8.

[17] V. Ivády, G. Barcza, G. Thiering, S. Li, H. Hamdi, J.-P. Chou, Ö. Legeza, A. Gali, Ab initio theory of the negatively charged boron vacancy qubit in hexagonal boron nitride, Npj Comput. Mater. 6 (1) (2020) 1–6.

[18] E. Igumbor, R.E. Mapasha, W.E. Meyer, Ab-initio study of aluminium impurity and interstitial-substitutional complexes in Ge using a hybrid functional (HSE), J. Electron. Mater. (2016) 1–8.

[19] E. Igumbor, G. Dongho-Nguimdo, R. Mapasha, E. Omotoso, W. Meyer, Stability, electronic and defect levels induced by substitution of Al and P pair in 4H–SiC, J. Phys. Chem. Solids 142 (2020) 109448.

[20] Y. Liao, G. Wang, J. Wang, K. Wang, S. Yan, Y. Su, Nitrogen vacancy induced in situ g-C3N4 pn homojunction for boosting visible light-driven hydrogen evolution, J. Colloid Interface Sci. 587 (2020) 110–120.

[21] J.M. Johnson, Z. Chen, J.B. Varley, C.M. Jackson, E. Farzana, Z. Zhang, A.R. Arehart, H.-L. Huang, A. Genc, S.A. Ringel, et al., Unusual formation of point-defect complexes in the ultrawide-band-gap semiconductor β- Ga 2 O 3, Phys. Rev. X 9 (4) (2019) 041027.

[22] H. Xiang, J. Zhang, F. Ren, R. Zhu, Y. Jia, C. Liu, Defect-complex engineering to improve the optoelectronic properties of Cu In S 2 by phosphorus incorporation, Phys. Rev. Appl. 19 (6) (2023) 064036.

[23] K. Dabsamut, A. Boonchun, W.R. Lambrecht, Computational study of defect complexes in β-LiGaO2 and their relation to the donor–acceptor-pair recombination, J. Appl. Phys. 133 (22) (2023).

[24] E. Igumbor, G. Dongho-Nguimdo, R.E. Mapasha, W.E. Meyer, Electronic properties and defect levels induced by group III substitution–interstitial complexes in Ge, J. Mater. Sci. 54 (15) (2019) 10798–10808.

[25] E. Igumbor, E. Omotoso, S.M. Tunhuma, H.T. Danga, W.E. Meyer, Rare earth substitutional impurities in germanium: A hybrid density functional theory study, Nucl. Instruments Methods Phys. Res. Sect. B: Beam Interactions Mater. Atoms 409 (2017) 31–35.

[26] H.-C. Lu, J.-I. Lo, Y.-C. Peng, B.-M. Cheng, Photoluminescence of diamond containing nitrogen vacancy defects as a sensor of temperature upon exposure to vacuum-and extreme-ultraviolet radiation, Phys. Chem. Chem. Phys. 22 (46) (2020) 26982–26986.

[27] E. Igumbor, O. Olaniyan, R.E. Mapasha, H.T. Danga, E. Omotoso, W.E. Meyer, Induced defect levels of P and Al vacancy-complexes in 4H-SiC: A hybrid functional study, Mater. Sci. Semicond. Process. 89 (2019) 77–84.

[28] M.A. Reshchikov, Photoluminescence from vacancy-containing defects in GaN, Phys. Status Solidi (A) 220 (10) (2023) 2200402.

[29] E.C. Prima, J. Manopo, E. Suhendi, A. Setiawan, G. Shukri, M.K. Agusta, B. Yuliarto, The effect of CuZn+ ZnCu defect complex on Cu2ZnSnS4 thin film solar cell: A density functional theory study, Mater. Chem. Phys. 296 (2023) 127192.

[30] Y. Yang, W. Guo, Y. Zhai, Q. Jin, H. Zhao, R. Zhang, Y. Liu, Oxygen-doped and nitrogen vacancy co-modified carbon nitride for the efficient visible light photocatalytic hydrogen evolution, New J. Chem. 44 (38) (2020) 16320–16328.

[31] R.E. Mapasha, E. Igumbor, N.F. Andriambelaza, N. Chetty, Electronic properties of vacancies in bilayer graphane, Phys. B 573 (2019) 67–71.

[32] J. Bhang, D. Yim, H. Ma, G. Galli, H. Seo, A carbon dimer defect as a spin qubit candidate in hexagonal boron nitride: an ab-initio study, Bull. Am. Phys. Soc. 65 (2020).

[33] A.M.Z. Tan, C. Freysoldt, R.G. Hennig, First-principles investigation of charged dopants and dopant-vacancy defect complexes in monolayer Mo S 2, Phys. Rev. Mater. 4 (11) (2020) 114002.

[34] J.R. Reimers, A. Sajid, R. Kobayashi, M.J. Ford, Understanding and calibrating density-functional-theory calculations describing the energy and spectroscopy of defect sites in hexagonal boron nitride, J. Chem. Theory Comput. 14 (3) (2018) 1602–1613.

[35] C. Huan, Y. Cai, D.R. Kripalani, K. Zhou, Q. Ke, Abnormal behavior of preferred formation of the cationic vacancies from the interior in a γ-GeSe monolayer with the stereo-chemical antibonding lone-pair state, Nanoscale Horizons 8 (3) (2023) 404–411.

[36] C. Huan, P. Wang, B. He, Y. Cai, Q. Ke, Oxygen deficient α-MoO 3 with enhanced adsorption and state-quenching of H 2 O for gas sensing: a DFT study, J. Mater. Chem. C 10 (5) (2022) 1839–1849.

[37] E. Marinho, C.R. Leão, Molybdenum defect complexes in bismuth vanadate, Phys. Chem. Chem. Phys. 22 (28) (2020) 16277–16285.

[38] A. Khanam, A. Vohra, J. Slotte, I. Makkonen, R. Loo, G. Pourtois, W. Vandervorst, A demonstration of donor passivation through direct formation of V-As i complexes in As-doped Ge1- x Sn x, J. Appl. Phys. 127 (19) (2020) 195703.

[39] J. Davidsson, V. Ivády, R. Armiento, T. Ohshima, N. Son, A. Gali, I.A. Abrikosov, Identification of divacancy and silicon vacancy qubits in 6H-SiC, Appl. Phys. Lett. 114 (11) (2019) 112107.

[40] B. Breeze, C. Meara, X. Wu, C. Michaels, R. Gupta, P. Diggle, M. Dale, B. Cann, T. Ardon, U. D'Haenens-Johansson, et al., Doubly charged silicon vacancy center, Si-N complexes, and photochromism in N and Si codoped diamond, Phys. Rev. B 101 (18) (2020) 184115.

[41] J.N. Baker, P.C. Bowes, J.S. Harris, R. Collazo, Z. Sitar, D.L. Irving, Complexes and compensation in degenerately donor doped GaN, Appl. Phys. Lett. 117 (10) (2020) 102109.

[42] D. Colleoni, A. Pasquarello, Oxygen defects in GaAs: A hybrid functional study, Phys. Rev. B 93 (12) (2016) 125208.

[43] C.J. Meara, M.J. Rayson, P.R. Briddon, J.P. Goss, Density functional investigation of boron incorporation in silicon-vacancy complexes, Diam. Relat. Mater. 109 (2020) 108016.

[44] D.J. Coxon, M. Staniforth, B.G. Breeze, S.E. Greenough, J.P. Goss, M. Monti, J. Lloyd-Hughes, V.G. Stavros, M.E. Newton, An ultrafast shakedown reveals the energy landscape, relaxation dynamics, and concentration of the N3vh0 defect in diamond, J. Phys. Chem. Lett. 11 (16) (2020) 6677–6683.

[45] X. Yan, B. Wang, H. Yan, C. Huan, Y. Cai, Q. Ke, Orbital hybridization and defective states of vacancy defects in AlN, Mater. Today Commun. 39 (2024) 109063.

[46] X. Wang, M. Zhao, H. Bu, H. Zhang, X. He, A. Wang, J. Appl. Phys. 114 (19) (2013) 194305.

[47] A. Csóré, H. Von Bardeleben, J. Cantin, A. Gali, Phys. Rev. B 96 (8) (2017) 085204.

[48] J.B. Varley, A. Janotti, C. Franchini, C.G. Van de Walle, Role of self-trapping in luminescence and p-type conductivity of wide-band-gap oxides, Phys. Rev. B 85 (8) (2012) 081109.

[49] M. Huang, H. Li, S. Chen, Triple-site dopant-defect complexes in the mg-h-codoped gan: First-principles identification, Phys. Status Solidi (A).
[50] H. Li, M. Huang, S. Chen, First-principles exploration of defect-pairs in GaN, J. Semicond. 41 (3) (2020) 032104.
[51] H. Koyama, K. Sueoka, Density functional theory study of stable configurations of substitutional and interstitial C and Sn atoms in Si and Ge crystals, J. Cryst. Growth 463 (2017) 110–115.
[52] V. Emtsev, N. Abrosimov, V. Kozlovski, D. Poloskin, G. Oganesyan, Interaction rates of group-III and group-V impurities with intrinsic point defects in irradiated Si and Ge, Semiconductors 52 (13) (2018) 1677–1685.
[53] J. Kujala, T. Südkamp, J. Slotte, I. Makkonen, F. Tuomisto, H. Bracht, Vacancy-donor complexes in highly n-type Ge doped with As, P and Sb, J. Phys.: Condens. Matter. 28 (33) (2016) 335801.
[54] E. Igumbor, M. Dongho-Nguimdo, E. Mapasha, R. Kalimuthu, A. Raji, W. Meyer, Trivalent atom defect-complex induced defect levels in germanium for enhanced Ge-based device performance, J. Electron. Mater. (2024) 1–10.
[55] J. Heyd, G.E. Scuseria, M. Ernzerhof, J. Chem. Phys. 118 (18) (2003) 8207–8215.
[56] G. Kresse, J. Furthmüller, Phys. Rev. B 54 (1996) 11169–11186.
[57] P.E. Blochl, Phys. Rev. B 50 (1994) 17953–17979.
[58] J.P. Perdew, K. Burke, M. Ernzerhof, Phys. Rev. Lett. 77 (1996) 3865–3868.
[59] F.J. Morin, J.P. Maita, Phys. Rev. 94 (1954) 1525–1529.
[60] H.J. Monkhorst, J.D. Pack, Phys. Rev. B 13 (1976) 5188–5192.
[61] S.B. Zhang, J.E. Northrup, Phys. Rev. Lett. 67 (1991) 2339–2342.
[62] E. Igumbor, C. Ouma, G. Webb, W. Meyer, Ab-initio study of germanium di-interstitial using a hybrid functional (HSE), Phys. B 480 (2016) 191–195.
[63] E.J. Baerends, Chemical potential, derivative discontinuity, fractional electrons, jump of the Kohn–Sham potential, atoms as thermodynamic open systems, and other (mis) conceptions of the density functional theory of electrons in molecules, Phys. Chem. Chem. Phys. 24 (21) (2022) 12745–12766.
[64] Y. Kumagai, F. Oba, Phys. Rev. B 89 (2014) 195205.
[65] E. Igumbor, et al., Hybrid Functional Study of Point Defects in Germanium (Ph.D. thesis), University of Pretoria, 2017.
[66] R. Mapasha, E. Omotoso, Electronic properties and defect levels induced by n/p-type defect-complexes in Ge, Mater. Sci. Semicond. Process. 150 (2022) 106906.